International Journal of
INTELLIGENT SYSTEMS AND APPLICATIONS IN ENGINEERING
ISSN:2147-6799 www.ijisae.org Original Research Paper

An Improved Method for Cholesterol Detection Using Iris Analysis

[1]Poovayar Priya M, [2]Ezhilarasan M

Submitted: 28/01/2024 **Revised**: 06/03/2024 **Accepted**: 14/03/2024

Abstract*:* The presence of cholesterol in the iris can be detected in the cornea area which is a whitish ring-shape. It is a sign of hyperlipidemia and is also correlated with coronary heart disease (CHD). Iridology is an alternative method to detect the presence of cholesterol in the iris. We proposed a novel method of detecting the presence of cholesterol using image processing techniques. In this method, the iris is segmented from the eye, enhancing of iris, then normalization of the iris, and then cholesterol detection using the Modified Daugman method was implemented. This method involves 3 stages of cholesterol detection. The result showed an impressive result in the detection of the presence of cholesterol when applying the iris code of different bits.

Keywords**:** Cholesterol, Modified Daugman method, Iridology, Iris segmentation, Iris enhancement, Iris normalization, Iris, heart disease.

1. Introduction

Iridology improves our capacity to perceive and comprehend our inner selves. The world within contains an incredible amount of life, energy, and power in all of its pulsating, brilliant tapestry of dynamic activity, living, moving chemistry, amazing cellular metabolism processes, and waves of absorption and elimination. Our physical form is very miraculous.

Iridology is a language that all people of all ages, races, and cultures can understand. To those who learn the language and study the markings about the individual, the iris unveils its mysteries. It's not long before one notices that each case of arthritis is distinct since iridology reveals the underlying etiology of the disease in each individual. Because the practitioner can precisely prescribe what each patient requires based on the interpretation of their iridology, treatment is particularly effective. A highly potent remedy is doing the right thing at the right moment.

The sodium ring, also known as the calcium ring, cholesterol ring, circulatory ring, hyper cholesterol ring, lypaemic diathesis constitutional type, or the arteriosclerosis ring in Fig. 1, is a subject of debate among iridologists. The ring can be hereditary, develop from bad lifestyle choices, or result from consuming too much salt from food, drink, soil, water, or medications. Calcium that is out of solution or an overabundance of cholesterol deposits could be the cause[1].

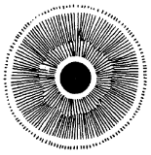

Fig. 1 Cholesterol ring

The ability to superimpose zones on normal analytic charts has been one of the useful developments of iris charts. In Fig. 2, there are seven zones:

I. The stomach region

2. Intestinal area

3. The pancreas, kidneys, solar plexus, heart, and aorta

4. Pituitary gland and bronchial tubes. pineal gland

5. Reproductive organs and the brain

6. Liver, thyroid, and spleen

7. Sweat glands, skin, lymphatic and circulatory systems. sensory and motor neurons

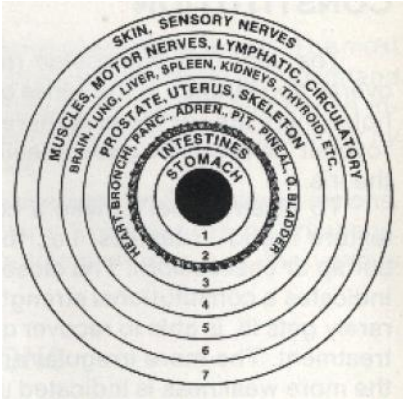

Fig.2 Seven Zones of Iris

Cholesterol ring: This unique sign, which begins in Zone 7, is a translucent-to-opaque ring that appears in different

[1]*Research Scholar Dept. of Computer Science and Engineering Puducherry Technological University, City: Puducherry -605014 Country: INDIA*
E-mail ID: poovayarpriya25@gmail.com
[2]*Professor Dept. of Information Technology Puducherry Technological University, City: Puducherry-605014 Country: INDIA*
E-mail ID: mezhil@ptuniv.edu.in

colors of white. appears to be a deposit or settlement around the perimeter of the area of the cornea that is seen in front of the iris in Figure 3, not touching the iris. In other words, it covers the iris without attaching to the iris trabeculae. The degree of the illness affects how wide it is. This indication is caused by chemical imbalances in the body as a result of medications like sodium salicylate that cause calcium to become out of solution and excessive salt or bicarbonate of soda use. and elevated blood triglycerides or cholesterol [2].

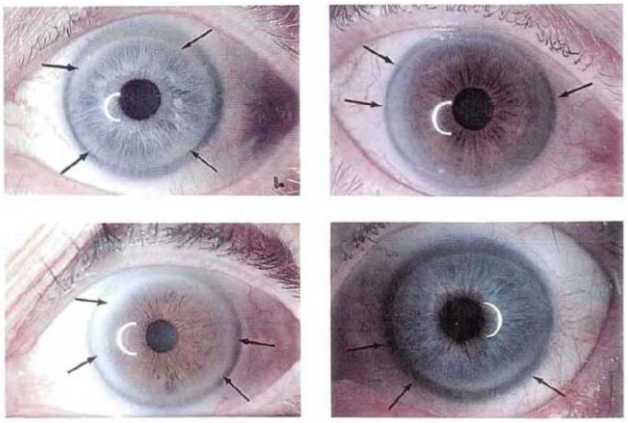

Fig.3 Cholesterol ring in Iris

The three stages of the disease are:

1. Incubation period: The first stage, where the white color appears on zone 7 appears mildly.
2. Prodromal stage: The second stage, where half of the white color surrounds zone 7.
3. Illness: The third stage, where the full white color is in zone 7.

2. Existing Methods

2.1 CA-Net model

To achieve a more accurate and comprehensible medical picture segmentation, Ran Gu [3] has created a comprehensive attention-based CNN (CA-Net) that makes use of multiple attentions in the CNN architecture. By concentrating on the most relevant scales and channels, the segmentation performance can be improved. CA-Net offers a detailed explanation of how each geographic location, feature map channel, and scale is used for prediction during segmentation tasks. The following is the definition of the Average Symmetric Surface Distance (ASSD), which is utilized in ground truth and automatic segmentation:

$$ASSD = \frac{1}{|S_a| + |S_b|} \times \left(\sum_{a \in S_a} d(a, S_b) + \sum_{b \in S_b} d(b, S_a) \right)$$

This network performs far more efficiently and is explainable than earlier methods. The Dice score produced by the CA-Net method was 92.08%. In the future, this method can also be easily extended to segment 3D images.

2.2Attention U-Net

Ozan Oktay et al. [4] introduced attention gates that are incorporated into the standard U-Net architecture in order to draw attention to the important components that are transported into the skip connections. Information gated from the coarse scale helps to separate out the noisy responses from the irrelevant ones in skip connections. This is carried out just before concatenation to guarantee that only relevant activations are joined. Furthermore, AGs filter activations of neurons during both the forward and reverse passes. The backward pass involves down-weighting the gradients that start in background areas. This allows for the updating of model parameters depending on the locations of shallower layers' spatial regions. The following is one way to design the update rule for the layer l convolution parameters:

$$\frac{\partial(\hat{x}_i^l)}{\partial(\Phi^{l-1})} = \frac{\partial\left(\alpha_i^l f(x_i^{l-1}; \Phi^{l-1})\right)}{\partial(\Phi^{l-1})} = \alpha_i^l \frac{\partial(f(x_i^{l-1}; \Phi^{l-1}))}{\partial(\Phi^{l-1})} + \frac{\partial(\alpha_i^l)}{\partial(\Phi^{l-1})} x_i^l$$

2.3 LinkNet model

LinkNet is a light deep neural network architecture for semantic segmentation, useful for augmented reality and self-driving car projects. Yooseung Wang et al. [5] proposed NL-LinkNet, which has the ability to identify connections between global properties. This allows for more accurate road segmentation by enabling each spatial feature point to utilize all other contextual data. Specifics: Without any postprocessing, such as conditional random field (CRF) refinement, this single model surpassed all other published state-of-the-art ensemble models in the official DeepGlobe Challenge. Further, our nonlocal LinkNet (NL-LinkNet) performed better with 43% fewer parameters, less giga floating-point operations per second (GFLOPs), and a faster training convergence time than the DeepGlobe challenge winner, D-LinkNet.

2.4 Retinex model

Non-local mean filtering and multi-scale Retinex were proposed by Zhenghau Chen[6]. First, NLM filtering reduces the problem of speckle noise for texture improvement. The MSR is then added to the filtered SAR image to improve the textural aspects of the oceanic internal waves. Real SAR photos from the Gaofen-3 satellite were used in the experiment to improve the textural features of oceanic internal wave

SAR images. The results demonstrate that the proposed method may effectively reduce image noise while significantly improving internal wave texture.

2.5 Histogram Equalization Method

Histogram equalization (HE) is an image processing technique used to enhance contrast in images. The core idea of HE is to modify the pixel values in an image to achieve a more uniform distribution over the entire possible value range [7]. Creating the image's histogram, or a graphical representation of how frequently each pixel value appears in the image, is the first stage in the HE process [8]. The histogram is then equalized by redistributing the pixel values to provide a more consistent distribution of values over the whole range of possible values [9].

2.6 AHE Method

An image's contrast can be improved by using Adaptive Histogram Equalization (AHE), a variant of the histogram equalization approach, especially in regions with low contrast or uneven illumination [10]. AHE applies distinct equalization functions to various picture regions depending on the local image statistics, in contrast to normal histogram equalization, which applies the same equalization function to the entire image. The AHE procedure is partitioning the image into discrete areas, or tiles, determining the histogram of each tile, and subsequently independently equalizing each histogram. This guarantees that contrast enhancement is applied only to the areas of the image that need it. One of the main advantages of AHE is that it maintains the local contrast of the image while improving overall contrast. For this reason, it is particularly useful for pictures having intricate textures, like satellite or medical photos [11].

2.7 CLAHE Method

Contrast Limited Adaptive Histogram Equalization (CLAHE) is a technique that can enhance an image's contrast while preventing artifacts such as the "halo effect" that may occur with Adaptive Histogram Equalization (AHE) [12]. Classical AHE has the potential to over-enhance contrast in image regions with a narrow histogram [13]. A prominent grid-like pattern around the borders, known as the "halo effect," may result from artifacts and noise in some places being amplified too much. CLAHE circumvents this limitation by limiting the contrast enhancement in each image tile. The "clip limit" is a predetermined figure that is used to clip the histogram to limit it. This prevents noise and artifacts from being amplified excessively and guarantees that contrast enhancement in regions with a narrow histogram is not overdone.

3. Materials and methods

3.1 Datasets

A college database called PEC datasets contains iris scans of students for research purposes. The 30 photographs in this collection comprise PNG files of the left and right iris images for every subject. All of the pictures are taken with an L1 solution sensor and near-infrared lighting. This clever design allows our iris camera to capture remarkably clear iris photos [15].

3.2 Segmentation of Iris

Using the Iris U-Net method[15], the iris portion of the eye picture is automatically separated in this work, as illustrated in Figure 4. Data from the datasets were randomly selected to provide training for twenty participants and testing for five subjects. From start to finish, this network is entirely convolutional. (FCN). It can accommodate images of any size because it does not have fully connected thick layers. The provided image has dimensions of 128 * 128 * 3. The accompanying graphic shows the left contractor path and the right extension path. Contractor Path extracts information from the image using convolution layers and max pooling layers. On the right side, transposed convolutional layers are combined with conventional convolutions to achieve this.

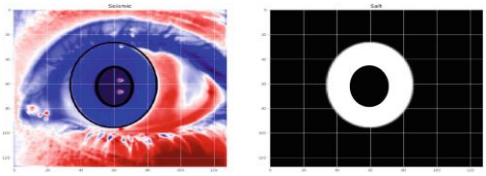

Fig.4 Iris segmentation

3.3 Enhancement of Iris

Using the SSR [14] approach in conjunction with CLAHE [12], iris enhancement was carried out. Training and testing data were taken from the following sets of subjects: 70 from the CASIA dataset, totaling 4035 images with 320*280 resolution in.jpeg format; 46 from the MMU dataset, totaling 460 images with 320*240 resolution in.bmp format; and 140 from the PEC dataset, totaling 450 images with 640*480 resolution in.png format. The CLAHE model only improves the local characteristics of iris pictures. However, when CLAHE and SSR are combined, local and global features are extracted, producing more enticing results, as seen in Fig. 5.

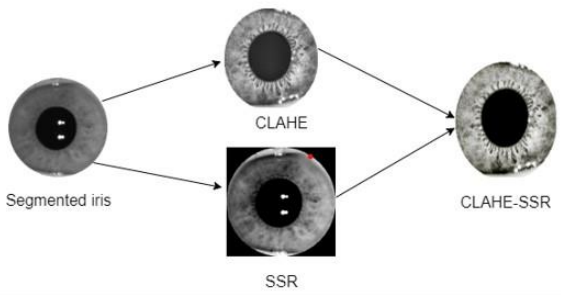

Fig.5 Iris enhancement

3.4 Normalization of Iris

The iris region is reshaped to have set dimensions during the normalization process. Dilation can also result from head tilt, camera rotation, eye rotation, and changes in image distance. An effective normalizing procedure should yield distinct iris regions for distinct iris types under identical settings as well as consistent dimensions for identical iris types under various conditions. The remap of each iris region's point to the polar coordinates (r,) in Figure 6 can be explained using Daugman's rubber-sheet model.

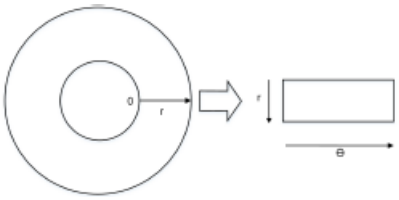

Fig. 6 Iris normalization

3.5 Detection of cholesterol

In the Daugman method [16], a 1-bit iris code is used for iris recognition. We have taken different bits for detecting the presence of cholesterol. For detecting the presence of cholesterol in the iris, after normalization of the iris, we have divided the normalized image into 7 zones given by [2]. Then we took the 7^{th} zone in the iris image and processed the image. We have detected the presence of cholesterol in three stages. In the incubation stage of the detection of cholesterol, a 2-bit representation of iris code is implemented as follows:

Step 1: The normalized iris is divided into 7 rows. The 7^{th} row was taken for the detection of cholesterol in the iris.

Step 2: Divide the grayscale pixel values into four intensity levels.

Step 3: Assign a 2-bit code to each intensity level: 00 for the first interval, 01 for the second interval, 10 for the third interval, and 11 for the fourth interval.

Step 4: For each pixel in the iris image, determine its intensity level based on the quantization intervals.

Step 5: Assign the corresponding 2-bit code to each intensity level and concatenate these codes to form the iris code.

In the prodromal stage of the detection of cholesterol, a 3-bit representation of the iris code is implemented as follows:

Step 1: The normalized iris is divided into 7 rows. The 7^{th} row was taken for the detection of cholesterol in the iris.

Step 2: Divide the grayscale pixel values into eight intensity levels.

Step 3: Assign a 3-bit code to each intensity level: 000 for the first interval, 001 for the second interval, and so on up to 111 for the eighth interval.

Step 4: For each pixel in the iris image, determine its intensity level based on the quantization intervals.

Step 5: Assign the corresponding 3-bit code to each intensity level and concatenate these codes to form the iris code.

In the illness stage of the detection of cholesterol, a 4-bit representation of the iris code is implemented as follows:

Step 1: The normalized iris is divided into 7 rows. The 7^{th} row was taken for the detection of cholesterol in the iris.

Step 2: Divide the grayscale pixel values into sixteen intensity levels.

Step 3: Assign a 4-bit code to each intensity level: 0000 for the first interval, 0001 for the second interval, and so on up to 1111 for the sixteenth interval.

Step 4: For each pixel in the iris image, determine its intensity level based on the quantization intervals.

Step 5: Assign the corresponding 4-bit code to each intensity level and concatenate these codes to form the iris code.

4. Results and Discussion

4.1 Incubation stage

Fig. 7 illustrates samples of the iris at the early stage of the presence of cholesterol. We have taken 30 samples of iris images, from which zone 7 is extracted. Fig. 8 represents the presence of cholesterol detection in iris images.

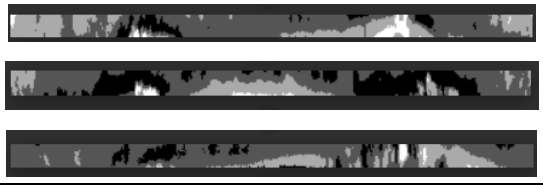

Fig. 7 Incubation stage

```
Cholesterol found in image: 1000.png
Cholesterol found in image: 1001.png
Cholesterol found in image: 1002.png
Cholesterol found in image: 1003.png
Cholesterol found in image: 1004.png
Cholesterol found in image: 1005.png
Cholesterol found in image: 1006.png
Cholesterol found in image: 1007.png
Cholesterol found in image: 1008.png
Cholesterol found in image: 1009.png
Cholesterol found in image: 1010.png
Cholesterol found in image: 1011.png
Cholesterol found in image: 1012.png
Cholesterol found in image: 1013.png
Cholesterol found in image: 1014.png
Cholesterol found in image: 1015.png
Cholesterol found in image: 1016.png
Cholesterol found in image: 1017.png
Cholesterol found in image: 1018.png
Cholesterol found in image: 1019.png
Cholesterol found in image: 1020.png
Cholesterol found in image: 1021.png
Cholesterol found in image: 1022.png
Cholesterol found in image: 1023.png
```

Fig. 8 Incubation stage with cholesterol detection

4.2 Prodromal stage

Fig. 9 illustrates samples of the iris at the next stage of the presence of cholesterol. We have taken 30 samples of iris images, from which zone 7 is extracted. Fig. 10 represents the presence of cholesterol detection in iris images.

Fig. 9 Prodromal stage

```
Cholesterol found in image: 1000.png
Cholesterol found in image: 1001.png
Cholesterol found in image: 1002.png
Cholesterol found in image: 1003.png
Cholesterol found in image: 1004.png
Cholesterol found in image: 1005.png
Cholesterol found in image: 1006.png
Cholesterol found in image: 1007.png
Cholesterol found in image: 1008.png
Cholesterol found in image: 1009.png
Cholesterol found in image: 1010.png
Cholesterol found in image: 1011.png
Cholesterol found in image: 1012.png
Cholesterol found in image: 1013.png
Cholesterol found in image: 1014.png
Cholesterol found in image: 1015.png
Cholesterol found in image: 1016.png
Cholesterol found in image: 1017.png
```

Fig. 10 Prodromal stage with cholesterol detection

4.3 Illness stage

Fig. 11 illustrates samples of the iris at the last stage of the presence of cholesterol. We have taken 30 samples of iris images, from which zone 7 is extracted. Fig. 12 represents the presence of cholesterol detection in iris images.

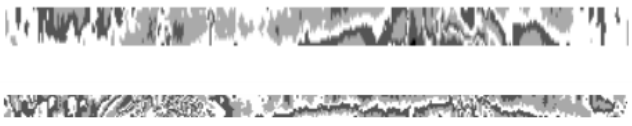

Fig. 11 Illness stage

```
Cholesterol found in image: 1000.png
Cholesterol found in image: 1001.png
Cholesterol found in image: 1002.png
Cholesterol found in image: 1003.png
```

Fig. 12 Illness stage with cholesterol detection

Fig. 13 scatter plot to show the distribution of pixel values across different representations. Random noise is added to the pixel values for better visualization separation. Scatter plots are created for each representation, with different colors to distinguish between them.

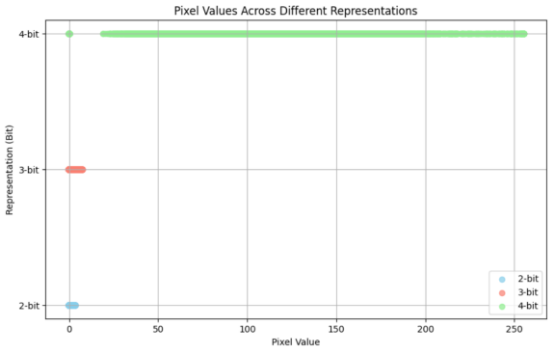

Fig. 13 Pixel value Vs bits

5. Conclusion

In this paper, we detected cholesterol presence using an image processing technique. First, we segmented the iris from eye images using the Iris U-Net model. Next, we applied an image enhancement technique to the iris image to bring a better quality of the iris. Then, we normalized the iris to extract zone 7 for the detection of cholesterol. The Daugman method was associated with a 1-bit representation of iris code. This method uses a modified Daugman method with different bits representation for different stages of cholesterol detection. The Experimental results showed an outperformance by detecting the presence of cholesterol in three stages of cholesterol detection. In the future, various diseases can be detected using Iridology.

References

[1] Sharan, F., 1989. *Iridology: A complete guide to diagnosing through the iris and to related forms of treatment*. HarperThorsons.

[2] Jensen B," Iridology simplified", California: Bernard Jensen, 1980.

[3] Gu, R., Wang, G., Song, T., Huang, R., Aertsen, M., Deprest, J., Ourselin, S., Vercauteren, T. and Zhang, S., 2020. CA-Net: Comprehensive attention convolutional neural networks for explainable

medical image segmentation. *IEEE transactions on medical imaging*, *40*(2), pp.699-711.

[4] Touvron, H., Cord, M., Douze, M., Massa, F., Sablayrolles, A. and Jégou, H., 2021, July. Training data-efficient image transformers & distillation through attention. In *International conference on machine learning* (pp. 10347-10357). PMLR.

[5] Wang, Y., Seo, J. and Jeon, T., 2021. NL-LinkNet: Toward lighter but more accurate road extraction with nonlocal operations. *IEEE Geoscience and Remote Sensing Letters*, *19*, pp.1-5.

[6] Chen, Z., Zeng, H., Yang, W. and Chen, J., 2022, November. Texture Enhancement Method of Oceanic Internal Waves in SAR Images Based on Non-local Mean Filtering and Multi-scale Retinex. In *2022 3rd China International SAR Symposium (CISS)* (pp. 1-5). IEEE.

[7] S. Agrawal, R. Panda, P. K. Mishro, and A. Abraham, ‘‘A novel joint histogram equalization based image contrast enhancement,’’ J. King Saud Univ.-Comput. Inf. Sci., vol. 34, no. 4, pp. 1172–1182, Apr. 2022, doi: 10.1016/j.jksuci.2019.05.010.

[8] B. S. Rao, ‘‘Dynamic histogram equalization for contrast enhancement for digital images,’’ Appl. Soft Comput., vol. 89, Apr. 2020, Art. no. 106114, doi: 10.1016/j.asoc.2020.106114.

[9] S. Doshvarpassand, X. Wang, and X. Zhao, ‘‘Sub-surface metal loss defect detection using cold thermography and dynamic reference reconstruction (DRR),’’ Struct. Health Monitor., vol. 21, no. 2, pp. 354–369, Mar. 2022, doi: 10.1177/1475921721999599.

[10] J. Murugachandravel and S. Anand, ‘‘Enhancing MRI brain images using contourlet transform and adaptive histogram equalization,’’ J. Med. Imag. Health Informat., vol. 11, no. 12, pp. 3024–3027, Dec. 2021, doi: 10.1166/jmihi.2021.3906.

[11] S. F. M. Radzi, M. K. A. Karim, M. I. Saripan, M. A. A. Rahman, N. H. Osman, E. Z. Dalah, and N. M. Noor, ‘‘Impact of image contrast enhancement on stability of radiomics feature quantification on a 2D mammogram radiograph,’’ IEEE Access, vol. 8, pp. 127720–127731, 2020, doi: 10.1109/ACCESS.2020.3008927.

[12] U. Kuran and E. C. Kuran, ‘‘Parameter selection for CLAHE using multi-objective cuckoo search algorithm for image contrast enhancement,’’ Intell. Syst. with Appl., vol. 12, Nov. 2021, Art. no. 200051, doi: 10.1016/j.iswa.2021.200051.

[13] M. R. Islam and M. Nahiduzzaman, ‘‘Complex features extraction with deep learning model for the detection of COVID19 from CT scan images using ensemble based machine learning approach,’’ Exp. Syst. Appl., vol. 195, Jun. 2022, Art. no. 116554, doi: 10.1016/j.eswa.2022.116554.

[14] Y. Yang, Z. Jiang, C. Yang, Z. Xia, and F. Liu, “Improved retinex image enhancement algorithm based on bilateral filtering,” in Proceedings of the 4th International Conference on Mechatronics, Materials, Chemistry and Computer Engineering 2015.

[15] Priyal, M.P. and Ezhilarasan, M., 2023, November. IRIS Segmentation Technique Using IRIS-UNet Method. In *Advanced Concepts for Intelligent Vision Systems: 21st International Conference, ACIVS 2023 Kumamoto, Japan, August 21–23, 2023 Proceedings* (Vol. 14124, p. 235). Springer Nature.

[16] Daugman, J., 2007. New methods in iris recognition. *IEEE Transactions on Systems, Man, and Cybernetics, Part B (Cybernetics)*, *37*(5), pp.1167-1175.